

ORIGINAL ARTICLE

Accelerated bone ingrowth by local delivery of Zinc from bioactive glass: oxidative stress status, mechanical property, and microarchitectural characterization in an ovariectomized rat model

Jbahi Samira^{1,2,3*}, Monji Saoudi², Kabir Abdelmajid⁴, Oudadesse Hassane¹, Rebai Treq⁴, Efeki Hafed², Elfeki Abdelfatteh¹ and Keskes Hassib⁴

¹Campus de Beaulieu, UMR CNRS 6226, University of Rennes, Rennes, France;

²Animal Ecophysiology Laboratory, Department of Life Sciences, Sfax Faculty of Science, University of Sfax, Sfax, Tunisia; ³Higher Institute of Applied Biology of Medenine, University of Gabes, Gabes, Tunisia; ⁴Histology, Orthopaedic and Traumatology Laboratory, Sfax Faculty of Medicine, University of Sfax, Sfax, Tunisia

Background: Synthetic bone graft substitutes such as bioactive glass (BG) material are developed in order to achieve successful bone regeneration. Zn plays an important role in the proper bone growth, development, and maintenance of healthy bones.

Aims: This study aims to evaluate *in vivo* the performance therapy of zinc-doped bioactive glass (BG-Zn) and its applications in biomedicine.

Methods: Female Wistar rats were ovariectomized. BG and BG-Zn were implanted in the femoral condyles of Wistar rats and compared to that of control group. Grafted bone tissues were carefully removed to evaluate the oxidative stress status, histomorphometric profile, mechanical property, and mineral bone distribution by using inductively coupled plasma optical emission spectrometry.

Results: A significant decrease of thiobarbituric acid-reactive substances was observed after BG-Zn implantation. Superoxide dismutase, catalase (CAT), and glutathione peroxidase (GPx) activities significantly increased in ovariectomized group implanted with Zinc-doped bioactive glass (OVX-BG-Zn) as compared to ovariectomized group implanted with bioactive glass (OVX-BG). An improved mechanical property was noticed in contact of OVX-BG-Zn (39 ± 6 HV) when compared with that of OVX-BG group (26 ± 9 HV). After 90 days of implantation, the histomorphometric analysis showed that trabecular thickness (Tb.Th) and trabecular number (Tb.N) were significantly increased with 28 and 24%, respectively, in treated rats of OVX-BG-Zn group as compared to those of OVX-BG groups. Trabecular separation (Tb.Sp) and trabecular bone pattern factor (Tb.Pf) were significantly decreased in OVX-BG-Zn group with 29.5 and 54% when compared with those of OVX-BG rat groups. On the other hand, a rise in Ca and P ion concentrations in the implanted microenvironment was shown and lead to the formation/deposition of Ca-P phases. The ratio of pyridinoline [Pyr] to dihydroxylysinoxaline [DHLNL] cross-links was normalized to the control level.

Conclusion: Our findings suggested that BG-Zn might have promising potential applications for osteoporosis therapy.

Keywords: zinc metallic ion; bioactive glass; osteoporosis; trabecular bone architecture; mechanical property; oxidative stress

Responsible Editor: Amin Bredan, VIB Inflammation Research Center & Ghent University, Belgium.

*Correspondence to: Jbahi Samira, Animal Ecophysiology Laboratory, Department of Life Sciences, Sfax Faculty of Science, University of Sfax, Sfax, Tunisia, Email: jbahisamira@yahoo.fr

Received: 18 May 2015; Revised: 23 July 2015; Accepted: 23 July 2015; Published: 19 October 2015

One zinc (Zn) content has been shown to decrease in aging, skeletal unloading, and postmenopausal conditions, suggesting its role in bone disorders (1). Zn metal has been demonstrated to have a stimulatory effect on osteoblastic bone formation and mineralization (2). Moreover, Zn has been shown to inhibit osteoclastic

bone resorption due to inhibiting osteoclast-like cell formation from bone marrow cells and stimulating apoptotic cell death of mature osteoclasts (3, 4). Furthermore, it has been shown to stimulate gene expression of the transcription factors runt-related transcription factor 2 (Runx2) that is related to differentiation into osteoblastic cells (5).

Postmenopausal osteoporosis is a kind of bone metabolic disease induced by estrogen deficiency. It is characterized by disequilibrium of bone formation and microarchitecture deterioration (6). Osteoporosis is often reflected by low bone mineral density (BMD) and fracture risk and affects the survival of bone marrow stromal cells and increased bone fragility. Ovariectomized (OVX) animal model is widely recognized to closely represent the pathophysiological situations of postmenopausal osteoporosis (7). Numerous treatments were available for reducing bone loss but each one had limitations. Despite the benefits of certain treatments such as selective estrogen receptor moderators, adverse outcomes such as increased risks for cancer have been identified (8). Because of their adverse effects, more attention has been focused on biomaterials among which, we distinguish bioactive glasses (BGs). In fact, recently, osteoporotic femur defect was used to evaluate the therapeutic effect of biomaterials or drug delivery in skeletal, metabolic, diseased environment, along with the advantages of easy handling and reliable surgical reproducibility (9).

BGs have been studied for use in a number of biomedical applications, including wound dressings, drug delivery systems, and other pharmaceutical applications (10–14). Melt-derived BGs are commercially available for bone repair in powder form (15). The cellular mechanism in which the BG demonstrates osteogenic response has been under extensive research. Numerous *in vitro* studies have shown that BGs stimulate the growth and maturation of osteoblasts, and they promote the expression and maintenance of the osteoblastic phenotype (16). Moreover, it has been demonstrated that BG stimulates multipotent bone marrow stromal cell functions (17). Formation of the Si-rich layer is known to be a crucial phase in bone bonding as it acts as a template for calcium phosphate precipitation (18). The calcium phosphate layer then directs new bone formation together with absorbing proteins (19). The extracellular proteins attract macrophages, and mesenchymal stem cells and osteoprogenitor cells. Subsequently, the osteoprogenitor cells proliferate and differentiate into matrix-producing osteoblasts. In order to determine whether a new material conforms to the requirements of biocompatibility and mechanical stability prior to clinical use, it must undergo rigorous testing under both initial *in vitro* and then *in vivo* conditions.

Different concentrations of Zn within BGs (BG-1.5 Zn and BG-5Zn) have been shown to affect bone-associated cell responses *in vitro* (20). When implanted in rat calvarial defects for 8 weeks, the BG-5Zn scaffolds showed a significantly better capacity to regenerate bone tissue compared to the non-doping scaffolds (21). Another study exhibited the cytocompatibility of a mesoporous BG scaffold containing 4% ZnO and the addition of Zn to BG was reported to elicit antimicrobial activity (21).

Our previous studies have been carried out in order to explore the effects of the BG-Zn biomaterial bioactivities by using *in vitro* analysis (22). A bone-like apatite layer formed on the surfaces of BG-Zn biomaterial after incubation in simulated body fluid (SBF) indicating BG-Zn bioactivity. The present study aims to investigate the *in vivo* antioxidant activity of Zn-doped BG against free radicals induced by estrogen deficiency, mechanical characterization, and trabecular bone architecture.

Materials and methods

Biomaterial synthesis

For elaboration of BGs, oxides (46 wt% SiO₂, 23.94 wt% CaO, 23.94 wt% Na₂O, 6 wt% P₂O₅, and 0.12 wt% ZnO) weighed and mixed in a polyethylene bottle for 2 h using a planetary mixer (23). This content of Zn is close to that of the human bone. The premixed mixtures were melted in platinum crucibles that were placed in an electric furnace. The first rise of temperature rate was 10°C/min and it was held at 900°C for 1 h to achieve the decarbonation of all products. The second rise of temperature rate was 20°C/min and it was held at 1,350°C for 3 h. The samples were casted in preheated brass cylindrical molds and annealed at 565°C for 4 h near the glass transition temperature of each glass. The prepared implants were sterilized by γ -irradiation from a 60 Co Source gamma irradiation, at a dose of 25 Gy (Equinox, UK), using standard procedures for medical devices.

Animals

Animal model

Female Wistar rats (16–19 weeks of age), obtained from the Central Pharmacy, Tunisia, and bred in the central animal house, were used in this study. The rats were acclimatized to their new environment for 7 days before the beginning of the study and were fed on a pellet diet (Sicco, Sfax, Tunisia) and water *ad libitum*. All of the animals were kept under climate-controlled conditions (25°C; 55% humidity; 12 h of light alternating with 12 h of darkness). The Tunisian ethical committee for the care and use of laboratory animals approved the handling of the animals. All rats were randomly divided into five groups (five animals per group). Group I was used as a negative control without bilateral ovariectomy or surgical creation of bone defects (CT). Sixty days after bilateral ovariectomy, Group II was used as a positive control; Ovariectomized (OVX), whereas, Group III was implanted with BG (OVX-BG). The last group (Group IV) was implanted with BG-Zn (OVX-BG-Zn).

Surgical and postoperative protocol

All surgical interventions were performed under general anesthesia in aseptic conditions. Anesthesia was induced

with xylazine (7–10 mg/kg (i.p.) ROMPUN2%, Merial; Lyon, France) and ketamine (70–100 mg/kg (i.m.) imalgene®, Merial; Lyon, France) depending on the body weight. The animals underwent bilateral ovariectomy. The pre-operative preparation of the surgical sites was routinely carried out by cleaning with 96% alcohol and antiseptic solutions (PROLABO; AnalaR Normapur®, France). A drilled 3-mm-diameter and 4-mm-deep hole was created on the lateral aspect of the femoral condyle using a refrigerated drill to avoid necrosis. The resulting bone defects were irrigated profusely with physiological saline solution (0.9 wt% NaCl; Ref. 091214; Siphall, Tunisia) to eliminate bone debris. BGs were implanted in the form of blocks. The drill hole was filled with 10 mg of BG and 10 mg of BG-Zn in OVX-BG and OVX-BG-Zn groups, respectively. The animals were sacrificed 30, 60, and 90 days postoperatively. The femoral condyles were exarticulated at the knee joint and freed from all adhering soft tissues.

Oxidative stress

Tissue preparation and stress oxidative

Thiobarbituric acid–reactive substance measurements

The femurs were removed and rapidly frozen by dry ice. The two tissues of all groups were minced and homogenized (100 mg/ml) at 4°C in 0.1 mol/l Tris-HCl buffer pH 7.4 and centrifuged at 3,000 g for 10 min. The implanted bone of all groups were minced and homogenized (100 mg/ml) at 4°C in 0.1 mol/l Tris-HCl buffer pH 7.4 and centrifuged at 3,000 g for 10 min. Lipid peroxidation in the tissue homogenate was estimated by measuring thiobarbituric acid–reactive substances (TBARS) and was expressed in terms of malondialdehyde (MDA) content which is the end product of lipid peroxidation (24).

Antioxidant enzyme studies

Regarding the superoxide dismutase (SOD) activity, it was assayed by the spectrophotometric method (25). Glutathione peroxidase (GPx) activity was measured by the method (26). Catalase (CAT) activity was assayed calorimetrically at 240 nm and expressed as moles of H₂O₂ consumed per minute per milligram of protein (27). The level of total protein was determined by the method of Lowry et al. (28) using bovine serum albumin.

Hardness measurement

The hardness was measured by using Vickers Tester. The Vickers hardness number: $HV = 2P \sin(h/2) / D^2$, where P is the applied load in kg, D is the mean length of the diagonals in mm, and h is the angle (136°) between opposite faces of the Diamond Pyramid. Measurements are taken after BG and BG-Zn bone implantation.

Histomorphometric evaluation

The implanted femoral condyles were harvested, fixed in Burdack (formalin), and refrigerated. Specimens were dehydrated using alcohol titrated solutions from 70 to 100% EtOH. Then, the specimens were infiltrated by methylmethacrylate that was allowed to polymerize, before placing it in a mixture of methylmethacrylate (MMA) and glycolmethacrylate (GMA), without prior decalcification. Using a sliding microtome (Reichert-Jung), sections of 6–7 μm thick were debited by cutting along a transverse plane. Moreover, the sections were stained with modified Goldner trichrome. The histomorphometric parameters were measured by a point count method (29) using a 25-point integrating filter.

Determination of bone mineral content using inductively coupled plasma optical emission spectrometry

Femurs were dried for 24 h at 65°C. Dry bones were weighed accurately and placed in 25-ml tubes; 2 ml of nitric acid was added. One milliliter of 30% H₂O₂ (Sigma) was placed in the tube after 10 min. The volume of the mixture was made up to 500 ml with distilled water. Standard solutions of Ca, P, Si, Zn, and Mg were used to prepare the working standard solution and a blank solution. The element concentrations were detected using inductively coupled plasma optical emission spectrometry (ICP-OES; Ciro; Spectro Analytical Instrument, Germany).

Cross-link

The newly formed bone was used to analyze the collagen cross-linking in the bone. The reduction of collagen in the callus was performed using sodium borohydride (NaBH₄, Sigma-Aldrich Japan K.K., Tokyo, France) and subsequent quantification of reducible immature and non-reducible mature pyridinium cross-links was carried out by high-performance liquid chromatography (HPLC) as previously described (30).

Statistical analysis

Statistical analysis was performed using Mann–Whitney U -test with SPSS software (Version 17.0). $P < 0.05$ was accepted as statistically significant.

Results

In vivo

Oxidative stress parameters

As illustrated in Fig. 1a–c, the data on the SOD, CAT and GPx activities in the bone of OVX rats showed a highly significant decrease when compared to those of control rats. Also, estrogen deficiency elevated the MDA levels (Fig. 1d). After 90 days of implantation, OVX-BG and OVX-BG-Zn groups showed a particular increase in SOD, CAT, and GPx activities when compared to OVX group and a significant decrease of MDA levels.

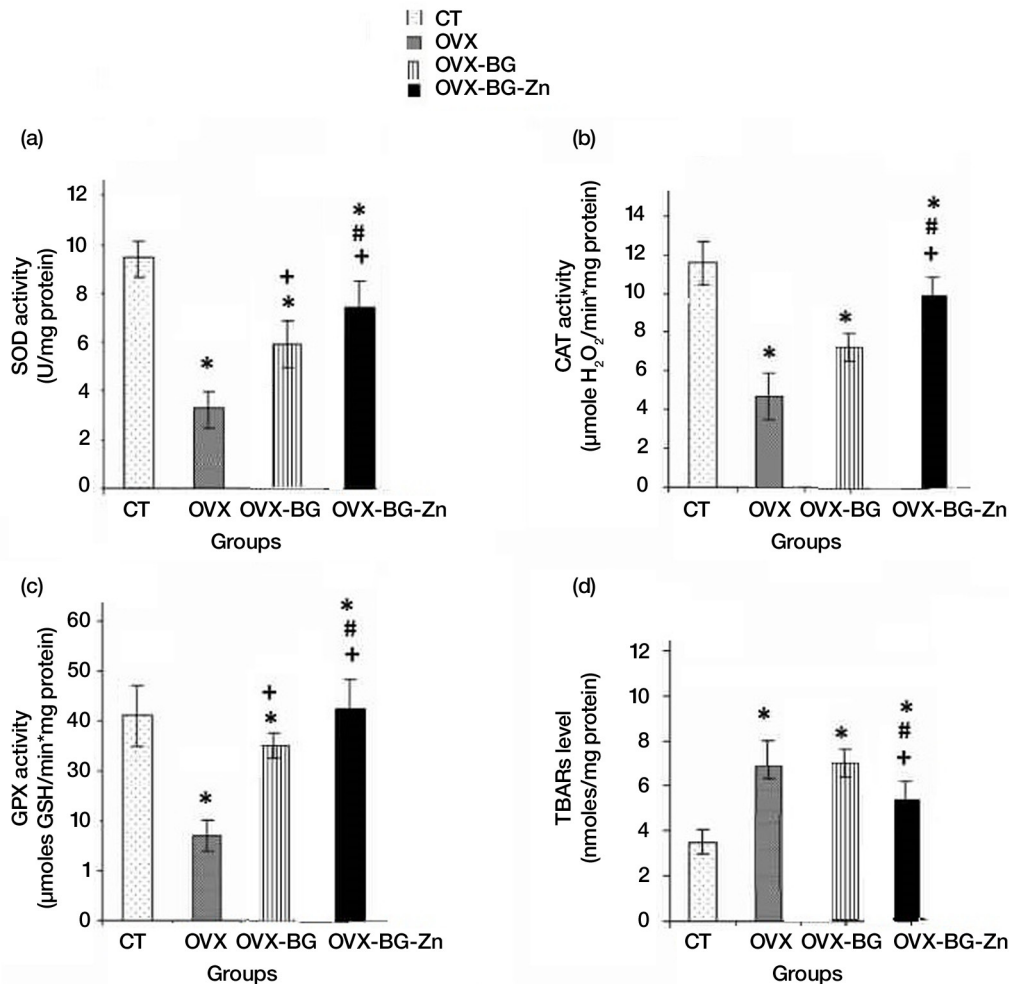


Fig. 1. Effects of bioactive glass (BG) and zinc-doped bioactive glass (BG-Zn) on superoxide dismutase (SOD) (a), catalase (CAT) (b) and glutathione peroxidase (GPx) (c) activities, thiobarbituric acid–reactive substances (TBARS) (d) in femoral condyle bone of ovariectomised female Wistar rats after 90 days. Values are given as means ± SE. Significantly less enzymatic activity in the indicated group versus the control group, ⁺versus the ovariectomized group (OVX) and [#]versus the ovariectomized group and implanted with bioactive glass (OVX-BG), [¥]versus the ovariectomized group and implanted with Zinc doped bioactive glass (OVX-BG-Zn).

This positive action was more pronounced in OVX-BG-Zn than that of OVX-BG. In fact, an increase in the SOD, CAT, and GPx activities in OVX-BG-Zn with 30, 42, and 20% respectively, was shown at the end of the experiment. Moreover, a decrease in MDA level by 40% was detected in OVX-BG-Zn as compared to the OVX-BG group. A significant enhancement of enzymatic defenses was observed especially in comparison with OVX group. A pronounced increase of the SOD, CAT, and GPx activities by 160, 105 and 320% respectively was shown in OVX-BG-Zn when compared to the OVX group. In the same way, an important decrease in MDA level by 40% was detected.

Biomechanical test

Table 1 shows the results of the hardness measurement in the femoral condyle bone, BG-Zn-bone and the

BG-bone after 30, 60, and 90 days of implantation. The BG-Zn-bone hardness measurement exhibited a similar transitional pattern to that of femoral condyle bone. It reached even higher levels after 90 days of implantation and it reached 39 ± 6 HV.

Enzymatic cross-links in bone

Fig. 2 shows the content of enzymatic cross-links in the bone callus before and after bone implantation. At the newly formed bone site, the total content of enzymatic cross-links (sum of immature forms and mature forms) and the total content of immature cross-links (sum of DHLNL, HLNL, and LNL) of callus bone in ovariectomized groups were significantly lower than in the normal group. Estrogen deficiency significantly affected the enzymatic cross-links of femoral bone. The contents of HLNL and LNL, which is the immature cross-links, and Dpyr,

Table 1. Bone hardness testing after 30, 60, and 90 days of implantation: ovariectomized rat (OVX), ovariectomized rat implanted with bioactive glass (OVX-BG), ovariectomized rat implanted with Zinc-doped bioactive glass (OVX-BG-Zn)

Hardness test (HV)	30 days	60 days	90 days
Control	37 ± 6 ^{§,¥,†}	38 ± 8 ^{§,¥}	38 ± 7 ^{§,¥}
OVX	8 ± 1 ^{*,¥,†}	9 ± 4 ^{*,¥,†}	8 ± 2 ^{*,¥,†}
OVX-BG	25 ± 4 ^{*,§,†}	26 ± 2 ^{*,§,†}	26 ± 9 ^{*,§,†}
OVX-BG-Zn	41 ± 7 ^{¥,§}	40 ± 1 ^{¥,§}	39 ± 6 ^{§,¥}

* $p < 0.01$ vs. control; [§] $p < 0.01$ vs. OVX group; [¥] $p < 0.01$ vs. OVX-BG group; [†] $p < 0.01$ vs. OVX-BG-Zn group. Values are expressed as means ± SD of five rats.

which is a mature crosslink, in the OVX-BG-Zn-treated group, were significantly higher than that of all other groups.

ICP-OES of newly formed bone

After ovariectomy, Ca, P, and Zn contents were significantly decreased in osteoporotic rats when compared to those of control group ($P < 0.01$) as illustrated in Table 2, whereas Mg did not show any significant differences in OVX-BG-Zn group when compared to those of control group. After 90 days of OVX-BG-Zn implantation, Ca concentration in rat femurs was comparable to the control group and revealed at about 295 mg/g. Similarly, the P content measurements showed at about 147 mg/g after 90 days in the OVX-BG-Zn group which was comparable to the control group (143 mg/g). Zn concentrations were normalized to the initial bone amount and revealed at about 0.78 mg/g for OVX-BG-Zn group.

Histological analysis

Histological evidence showed a healthy bone of control rat (Fig. 3a). After 60 days of ovariectomy, the femoral condyle defect was characterized with a disconnected trabecular tissue (Fig. 3b). The dominance of the osteoid and woven bone tissue was shown in contact of the OVX-BG implanted group (Fig. 3c). After about 90 days, the dominance of a mineralized tissue after BG-Zn biomaterial treatment was noticed (Fig. 3d). In this case, the implanted OVX-BG-Zn rat bones were compared to a healthy one without degradation of trabecular connectivity (Fig. 3e). In fact, OVX-BG-Zn was shown to limit bone loss inducing a beneficial impact on the trabecular bone microarchitectural properties when compared to those of OVX-BG-treated rats.

Histomorphometric analysis

After 90 days of implantation, the quantitative analysis demonstrated that Tb.Th and Tb.N were more significantly increased with 28 and 24% respectively, in treated OVX-BG-Zn group than those of OVX-BG rats. Tb.Sp and TBPf were significantly decreased in OVX-BG-Zn

group with 29.5 and 54% when compared with that of OVX-BG rat group (Table 3).

Discussion

Tissue engineering-based approach represents a promising alternative for traditional osteoporosis therapies (31). In this regard, considerable attention has been given to BGs which are suitable for bone regeneration applications as they bond with bone and can be tailored to release therapeutic ions.

In the present study, estrogen deficiency showed that the bone graft has weakened the antioxidative bone tissue capacity and led to oxidative stress. In fact, growing evidence shows that oxidative stress is involved in the pathogenesis of bone diseases, including osteoporosis (32). The processes of bone turnover are mediated by reactive oxygen species (ROS). Oxidative/reductive processes are an integral component of bone remodeling; however, an excessive production and accumulation of ROS in the bone tissue has detrimental impact on the bone metabolism (33, 34). ROS decrease bone formation by the inhibition of osteoblasts generation from osteoprogenitor cells and by the shortening of their survival (35). In the present study, after 90 days of implantation, the antioxidative stress parameters such as SOD, CAT, and GPx were enhanced following BG-Zn implantation. These findings suggest that BG-Zn is responsible for the strong antioxidant effect. In fact, SOD activity is dependent on Zn, Cu, and Mn elements (36, 37). In a recent study, Zn has been shown to protect from oxidative protein and DNA damage as well as lipid peroxidation and caused improvement of the bone tissue oxidative/antioxidative balance. On the other hand, the investigation of the mineral profile of the regenerated tissue showed that the bone remodeling behavior was attributed to the concentration of ions, such as Ca, P, and Si. In fact, the dissolution product of Si ion was demonstrated to promote osseointegration and mineralization in the initiation stage of bone tissue (36), as well as to facilitate angiogenesis investigated from both *in vitro* and *in vivo* studies (37). Ca ion can directly activate intracellular mechanisms by affecting Ca-sensing receptors in osteoblastic cells, followed by increasing the expression of insulin-like growth factors to regulate human osteoblast proliferation (38). Besides, inorganic phosphate is another essential element for hydroxyapatite deposition and bone matrix mineralization (39). The *in vivo* model keeps determining the true capacity of the improved materials to be appropriately used for bone regeneration. In the present study, after 60 days of ovariectomy, the femoral condyle defect was characterized with a disconnected trabecular tissue. Histological evidence showed a weakened bone after estrogen deficiency. However, BG-Zn administration is proposed to prevent the decrease in bone microarchitecture deterioration and bone loss associated

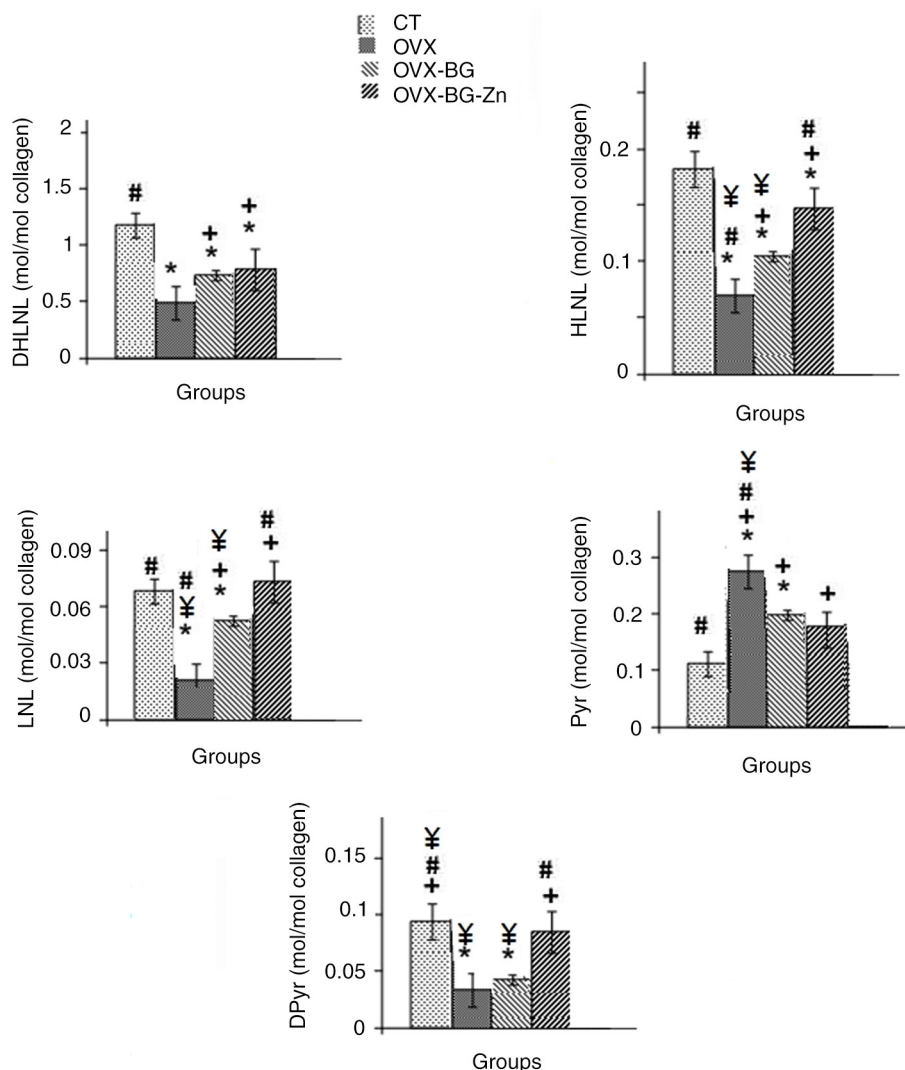


Fig. 2. Comparison of the contents of enzymatic collagen cross-links in femur of control rat, ovariectomized rat (OVX), ovariectomized and implanted with bioactive glass (OVX-BG), ovariectomized and implanted with Zinc doped bioactive glass (OVX-BG-Zn) *Significantly less enzymatic activity in the indicated group versus the control group, + versus the ovariectomized group (OVX) and # versus the ovariectomized group and implanted with bioactive glass (OVX-BG), † versus the ovariectomized group and implanted with zinc-doped bioactive glass (OVX-BG-Zn).

with postmenopausal osteoporosis. This *in vivo* study has a special focus on understanding the effect of Zn ion doping into BGs on mechanical properties. *In vivo*, it is

important that the biomaterial exhibits adequate mechanical strength because bone is under continuous stress (40). Thus, ideally the strength of implanted cell–biomaterial

Table 2. Distribution of Ca, P, Si, Zn, and Mg in control rat, ovariectomized rat (OVX), ovariectomized rat implanted with bioactive glass (OVX-BG), ovariectomized rat implanted with Zinc-doped bioactive glass (OVX-BG-Zn)

	Ca (mg)	P (mg)	Si (µg)	Zn (mg)	Mg (µg)
CT	310.00 ± 110	143.00 ± 67	27.00 ± 11 ⁺	0.68 ± 0.2 ⁺	4.7 ± 0.19
OVX	200.00 ± 70 ^{*+}	110.00 ± 70 ^{*+}	20.00 ± 9.0 ⁺	0.22 ± 0.08 ^{*+}	1.28 ± 0.50 ^{*+}
OVX-BG	252.00 ± 98 ^{*+}	142.10 ± 50	57.05 ± 20 [*]	0.27 ± 0.04 ^{*+}	3.99 ± 1.0
OVX-BG-Zn	295.00 ± 130 ⁺	147.70 ± 62	58.10 ± 19 [*]	0.78 ± 0.05	4.9 ± 0.70

**p* < 0.01 vs. control; ⁺*p* < 0.01 vs. OVX-BG-Zn group. Values are expressed as means ± SD of five rats.

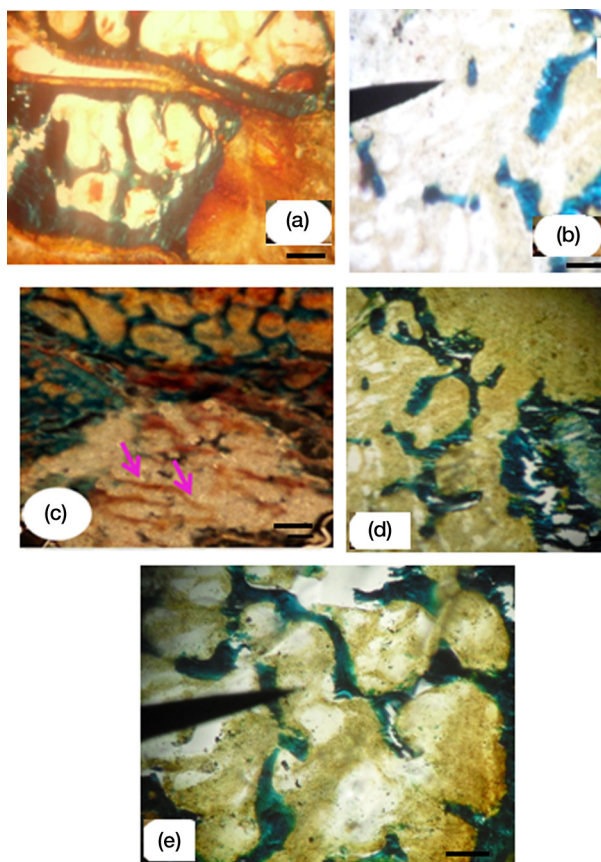


Fig. 3. The control groups in healthy bone (a), disconnected trabecular tissue in ovariectomized rat bone (b). Woven bone in OVX-BG group (c), mineralized bone implanted with BG-Zn in OVX-BG-Zn implanted group (d), and connected trabecular tissue in the OVX-BG-Zn implanted group after 90 days of implantation (e). (a, b and c, d, e Goldner's trichrome staining) ($10\times$ objective, scale bar = $20\ \mu\text{m}$).

construct should match that of living bone (41). The present study underscores that the Zn ion doping into BG network is a potential approach to enhance the mechanical properties. One of the explanations regarding mechanical enhancement is that after *in vivo* contact, a formation of thin needles of hydroxyapatite entangled

in the matrix was detected (42). In addition, BG-Zn increased the enzymatic cross-links in postmenopausal osteoporosis model. Of particular interest, in the BG-Zn-treated group, there was a high correlation between mechanical properties and enzymatic collagen cross-links, suggesting that an improvement in mechanical strength by BG-Zn administration is closely associated with an increase in enzymatic cross-links. In fact, bone quality is prescribed by the characteristic of the matrix (material quality) and the structural characteristic of bone. Material quality, including collagen cross-linking, plays an important role in the reinforcement of bone strength. In bone, enzymatic cross-links are considered to be beneficial because they have a positive effect on the physiological functions of bone. It was reported that Zn regulates collagen cross-linking and copper/zinc SOD causes bone fragility owing to low-turnover osteoporosis and impaired collagen cross-linking. Recently, it was observed that, in hip fracture, lysine hydroxylation of collagen chains increased, which was associated with significantly higher values of Pyr/Dpyr (43). In the present osteoporotic animal model, Zn may play a fundamental role in the collagen cross-linking process stability.

Conclusion

This study demonstrated that synthesized BG-Zn can be used as bone substitutes for local implantation into osteoporotic defects. In fact, the antioxidative stress parameters such as SOD, CAT, and GPx were enhanced after 90 days of implantation. The BG-Zn-bone hardness measurement exhibited a similar transitional pattern to that of femoral condyle bone. The histomorphometric parameters such as Tb.Th, Tb.N, Tb.Sp, and TBPf showed a significant amelioration. Concerning the enzymatic cross-links, the contents of HLNL and LNL, which is the immature cross-links, and Dpyr, which is a mature crosslink, were significantly enhanced in the OVX-BG-Zn-treated group. The investigation of the mineral profile of the regenerated tissue showed the deposition of significant amounts of mineralized matrix with a significant increase

Table 3. Determination of (Tb.Pf), (Tb.Th), (Tb.N), and (Tb.Sp) after 90 days in control femoral condyle Wistar rats (CT), ovariectomized rats (OVX), ovariectomized rat implanted with bioactive glass (OVX-BG), ovariectomized rat implanted with Zinc-doped bioactive glass (OVX-BG-Zn)

	Tb.Pf (/mm)	Tb.Th (μm)	Tb.N (/mm)	Tb.Sp (μm)
Control	$4.1 \pm 1^{\S}$	$176 \pm 25^{\S,\Psi}$	$1.2 \pm 0.4^{\S}$	$1,240 \pm 320^{\S,\Psi}$
OVX	$9.5 \pm 2^{*,\Psi,\dagger}$	$123 \pm 30^{*,\Psi,\dagger}$	$0.6 \pm 0.09^{*,\Psi,\dagger}$	$1,803 \pm 530^{*,\S,\Psi,\dagger}$
OVX-BG	$7.4 \pm 1^{\S,\dagger}$	$132 \pm 40^{*,\S,\dagger}$	$0.87 \pm 0.09^{\S,\dagger}$	$1,684 \pm 325^{*,\S,\dagger}$
OVX-BG-Zn	$4.8 \pm 1.55^{\S,\Psi}$	$169 \pm 62^{\S,\Psi}$	1.08 ± 0.09	$1,300 \pm 400^{\S,\Psi}$

* $p < 0.01$ vs. control; $^{\S}p < 0.01$ vs. OVX group; $^{\Psi}p < 0.01$ vs. OVX-BG group; $^{\dagger}p < 0.01$ vs. OVX -BG-Zn group. Values are expressed as means \pm SD of five rats.

in Ca-P layer. These data suggest the BG-Zn therapeutic approaches to bone diseases.

Conflict of interest and funding

No potential conflict of interest relevant to this article was reported.

References

- Sadeghi N, Oveisi MR, Jannat B, Hajimahmoodi M, Behzad M, Behfar F, et al. The relationship between bone health and plasma zinc, copper lead and cadmium concentration in osteoporotic women. *J Environ Health Sci Eng*. 2014; 1: 125.
- Li B, Liu H, Jia S. Zinc enhances bone metabolism in ovariectomized rats and exerts anabolic osteoblastic/adipocytic marrow effects ex vivo. *Biol Trace Elem Res*. 2014; 29: 202–7.
- Shepherd DV, Kauppinen K, Brooks RA, Best SM. An in vitro study into the effect of zinc substituted hydroxyapatite on osteoclast number and activity. *J Biomed Mater Res A*. 2014; 102: 4136–41.
- Rink L, Gabriel P. Extracellular and immunological actions of zinc. *Biometals*. 2001; 14: 367–83.
- Noman AS, Koide N, Iftakhar-E-Khuda I, Dagvadorj J, Tumurkhuu G, Naiki Y, et al. Retinoblastoma protein-interacting zinc finger 1 (RIZ1) participates in RANKL-induced osteoclast formation via regulation of NFATc1 expression. *Immunol Lett*. 2010; 131: 166–9.
- Kazantzis G. Cadmium, osteoporosis and calcium metabolism. *Biometals*. 2004; 17: 493–8.
- Jebahi S, Oudadesse H, Saoudi M, Kallabi F, Pascal P, Rebai T, et al. Cytocompatibility, gene-expression profiling, apoptotic, mechanical and ²⁹Si, ³¹P solid-state nuclear magnetic resonance studies following treatment with a bioglass chitosan composite. *Biotechnol Lett*. 2014; 36: 2571–9.
- Cordina-Duverger E, Truong T, Anger A, Sanchez M, Arveux P, Kerbrat P, et al. Risk of breast cancer by type of menopausal hormone therapy: a case-control study among post-menopausal women in France. *PLoS One*. 2013; 8: 78016.
- Su WT, Wu PS, Huang TY. Osteogenic differentiation of stem cells from human exfoliated deciduous teeth on poly(ϵ -caprolactone) nanofibers containing strontium phosphate. *Mater Sci Eng C Mater Biol Appl*. 2015; 46: 427–34.
- Jebahi S, Oudadesse H, El Feki H, Rebai T, Keskes H, Pascal P, et al. Antioxidative/oxidative effects of strontium-doped bioactive glass as bone graft, in vivo assays in castrated rats. *J Appl Biomed*. 2012; 10: 195–209.
- Jebahi S, Oudadesse H, Ben Saleh G, Saoudi M, Mesadhi S, Rebai T, et al. Chitosan-based bioglass composite for bone tissue healing: oxidative stress status and antiosteoporotic performance in a ovariectomized rat model. *Korean J Chem Eng*. 2014; 31: 1616–23.
- Nezafati N, Moztaazadeh F, Hesarakhi S. Surface reactivity and in vitro biological evaluation of sol gel derived silver/calcium silicophosphate bioactive glass. *Bioprocess Eng*. 2012; 17: 746–54.
- Jebahi S, Saoudi M, Farhat L, Oudadesse H, Rebai T, Kabir A, et al. Effect of novel curcumin-encapsulated chitosan–bioglass drug on bone and skin repair after gamma radiation: experimental study on a Wistar rat model. *Cell Biochem Funct*. 2015; 33: 150–9. doi: <http://dx.doi.org/10.1002/cbf.309>
- Anand V, Singh KJ, Kaur K. Evaluation of zinc and magnesium doped 45S5 mesoporous bioactive glass system for the growth of hydroxyl apatite layer. *J Non Cryst Solids*. 2014; 406: 88–94.
- Jones JR. Review of bioactive glass: from Hench to hybrids. *Acta Biomater*. 2013; 9: 4457–86.
- Xynos ID, Hukkanen MV, Batten JJ, Buttery LD, Hench LL, Polak JM. Bioglass 45S5 stimulates osteoblast turnover and enhances bone formation in vitro: implications and applications for bone tissue engineering. *Calcif Tissue Int*. 2000; 67: 321–9.
- Schepers EJ, Ducheyne P. Bioactive glass particles of narrow size range for the treatment of oral bone defects: a 1–24 month experiment with several materials and particle sizes and size ranges. *J Oral Rehabil*. 1997; 24: 171–81.
- Rabiee SM, Nazparvar N, Azizian M, Vashae D, Tayebi L. Effect of ion substitution on properties of bioactive glasses. *Ceram Int*. 2015; 41: 7241–51.
- Ducheyne P, Qiu Q. Bioactive ceramics: the effect of surface reactivity on bone formation and bone cell function. *Biomaterials*. 1999; 20: 2287–303.
- Wang H, Zhao S, Xiao W, Cui X, Huang W, Rahaman MN, et al. Three-dimensional zinc incorporated borosilicate bioactive glass scaffolds for rodent critical sized calvarial defects repair and regeneration. *Colloids Surf B Biointerfaces*. 2015; 130: 149–56.
- Sánchez-Salcedo S, Shruti S, Salinas AJ, Malavasi G, Menabue L, Vallet-Regí M. In vitro antibacterial capacity and cytocompatibility of SiO₂-CaO-P₂O₅ meso-macroporous glass scaffolds enriched with ZnO. *J Mater Chem B*. 2014; 2: 4836–47.
- Oudadesse H, Dietrich E, Gal YL, Pellen P, Bureau B, Mostafa A, et al. Apatite forming ability and cytocompatibility of pure and Zn-doped bioactive glasses. *Biomed Mater*. 2011; 6: 035006.
- Dietrich E, Oudadesse H, Lucas-Girot Y, Le Gal S, Cathelineau G. Effects of Mg and Zn on the surface of doped melt-derived glass for biomaterials applications. *Appl Surf Sci*. 2008; 255: 391–5.
- Buege JA, Aust SD. Microsomal lipid peroxidation. *Methods Enzymol*. 1984; 105: 302–10.
- Marklund S, Marklund G. Involvement of the superoxide anion radical in the autoxidation of pyrogallol and convenient assay for superoxide dismutase. *Eur J Biochem*. 1975; 47: 469–74.
- Pagila DE, Valentine WN. Studies on the quantitative and qualitative characterization of erythrocyte glutathione peroxidase. *J Lab Clin Med*. 1967; 70: 158–69.
- Aebi H. Catalase in vitro. *Methods Enzymol*. 1984; 105: 121–6.
- Lowry OH, Rosebrough NJ, Farr AL, Randall RJ. Protein measurement with Folin phenol reagent. *J Biol Chem*. 1951; 193: 265–75.
- Schenk RK, Merz WA, Müller JA. Quantitative histological study on bone resorption in human cancellous bone. *Acta Anat*. 1969; 74: 44–53.
- Cheng N, Wang Y, Zhang Y, Shi B. The osteogenic potential of mesoporous bioglasses/silk and non-mesoporous bioglasses/silk scaffolds in ovariectomized rats: in vitro and in vivo evaluation. *PLoS One*. 2013; 8: e81014. doi: <http://dx.doi.org/10.1371/journal.pone.0081014>
- Rabiee SM, Mortazavi J, Moztaazadeh F, Sharifi D, Fakhrejehani F, Khafaf A, et al. Association of a synthetic bone graft and bone marrow cells as a composite biomaterial. *Biotechnol Bioprocess Eng*. 2009; 14: 1–5.
- Brzóska MM, Rogalska J, Kupraszewicz E. The involvement of oxidative stress in the mechanisms of damaging cadmium action in bone tissue: a study in a rat model of moderate and relatively high human exposure. *Toxicol Appl Pharmacol*. 2011; 250: 327–33.
- Baek KH, Oh KW, Lee WY, Lee SS, Kim M, Kwon HS, et al. Association of oxidative stress with postmenopausal osteoporosis and the effects of hydrogen peroxide on osteoclast formation in human bone marrow cell cultures. *Calcif Tissue Int*. 2010; 87: 226–35.
- Kang KA, Chae S, Lee KH, Zhang R, Jung MS, You HJ, et al. Antioxidant effect of homogenetic acid on hydrogen peroxide

- induced oxidative stress in human lung fibroblast cells. *Biotechnol Bioprocess Eng.* 2005; 10: 556–63.
35. Arai M, Shibata Y, Pugdee K, Abiko Y, Ogata Y. Effect of reactive oxygen species (ROS) on antioxidant system and osteoblastic differentiation in MC3T3-E1 cells. *IUBMB Life.* 2007; 59: 27–33.
 36. Zreiqat H, Ramaswamy Y, Wu C, Paschalidis A, Lu Z, James B, et al. The incorporation of strontium and zinc into a calcium–silicon ceramic for bone tissue engineering. *Biomaterials.* 2010; 31: 3175–84.
 37. Lusvardi G, Zaffe D, Menabue L, Bertoldi C, Malavasi G, Consolo U. In vitro and in vivo behaviour of zinc-doped phosphosilicate glasses. *Acta Biomater.* 2009; 5: 419–28.
 38. Marie PJ. The calcium-sensing receptor in bone cells: a potential therapeutic target in osteoporosis. *Bone.* 2010; 46: 571–6.
 39. Wittrant Y, Bourguine A, Khoshniat S, Alliot-Licht B, Masson M. Inorganic phosphate regulates Glvr-1 and -2 expression: role of calcium and ERK1/2. *Biochem Biophys Res Commun.* 2009; 381: 259–63.
 40. Turan B, Bayari S, Balcik C, Severcan F, Akkas N. Biomechanical and spectroscopic study of bone from rats with selenium deficiency and toxicity. *Biomaterials.* 2000; 13: 113–21.
 41. Jebahi S, Ben Saleh G, Saoudi M, Besaleh S, Oudadesse H, Mhadbi M, et al. Genotoxicity effect, antioxidant and biomechanical correlation: experimental study of agarose–chitosan bone graft substitute in New Zealand white rabbit model. *J Eng Med.* 2014; 228: 800–9.
 42. Shuai C, Gao C, Feng P, Peng S, Wen X. Grain growth associates mechanical properties in nano-hydroxyapatite bone scaffolds. *J Nanosci Nanotechnol.* 2013; 13: 5340–5.
 43. Saito M, Shiraishi A, Ito M, Sakai S, Hayakawa N, Mihara M, et al. Comparison of effects of alfacalcidol and alendronate on mechanical properties and bone collagen cross-links of callus in the fracture repair rat model. *Bone.* 2010; 11: 70–9.